Geometry-Based Stochastic Channel Model for Train-to-Train Communication in Open Field Environment

Paul Unterhuber*, Michael Walter*, Thomas Kürner†
*Institute of Communications and Navigation, German Aerospace Center (DLR), Oberpfaffenhofen, 82234 Wessling, Germany, paul.unterhuber@dlr.de
†Institute for Communications Technology, Technische Universität Braunschweig, 38106 Braunschweig, Germany

***Abstract*—Future railway applications, e.g., wireless train bus or virtual coupled trains, will rely on train-to-train (T2T) communication. Those future applications require an exchange of safety critical data between trains within one train-set based on wireless communication. Hence, the investigation of the propagation effects and the influence on the wireless communication is tremendously important. Future developments of communication standards and systems demand a detailed characterization and modeling. We investigated the propagation mechanisms based on channel sounding measurements and derived statistics for the propagation effects. Based on the environment, geometry and the propagation statistics we derive channel models for T2T communication. To cope with the movement of the trains, the changing environment and resulting temporal correlation effects we present a geometry-based stochastic channel model (GSCM) for T2T communication in open field environment.**

***Index Terms*—train-to-train, high speed train, propagation, GSCM.**

I. Introduction

The future of railway communication will rely on a combination of train-to-ground (T2G) and T2T based communication. Novel railway applications like the wireless train bus, the concept of virtual coupled trains or fully autonomously driving trains will demand enhanced T2G and novel T2T communication [1]. Over the past decade, little attention has been paid to the area of research for T2T communication [2]. Within the frame work of the EU Horizon 2020 lighthouse project Roll2Rail the world-wide first T2T channel sounding measurements with two high speed trains were conducted in 2016 [3]. Since then, there have been less than a handful of other projects focused on T2T propagation.

Based on the collected channel sounding measurement data we derived propagation characteristics for typical railway environments like open field as presented in [4]. Furthermore, we analyzed the environment and extracted the influence of railway infrastructure on T2T propagation [5]. The most common elements along a electrified railway track are masts of the overhead line system. In addition we identified sparse cellular radio masts and trees as typical interacting objects (IOs) for an open field environment.

The movement of the trains, the geometry of the environment, the propagation effects of the environment, and the propagation effects of the IOs need to be represented by the T2T channel model. GSCMs are capable to fulfill the listed requirements and allow an investigation of temporal correlation effects for T2T communication. As a consequence, we present a GSCM for T2T communication and evaluate the GSCM with measurement data based on the power delay profile (PDP) and Doppler spectral density (DSD) for the open field environment.

II. Measurement Campaign

In 2016 we performed C-band measurements for a T2T communication link. We used the DLR RUSK channel sounder in single-input single-output (SISO) mode at a frequency of $f_\mathrm{c} = 5.2\,\mathrm{GHz}$. We recorded a discrete channel transfer function with a bandwidth of $B = 120\,\mathrm{MHz}$. The snapshot rate was set to $t_\mathrm{s} = 1.024\,\mathrm{ms}$ and the maximum excess delay t_p was set to $12.8\,\mu\mathrm{s}$. This measurement campaign was the world-wide first T2T channel sounder measurement campaign with two high speed trains. Trenitalia provided two Frecciarossa ETR 500 [6] high speed trains on the $205\,\mathrm{km}$ long high speed railway (HSR) track between Naples and Rome. The measurement equipment and setup was presented in more detail in [3].

III. Architecture of the Open Field Environment

We focus on an open field section of the high speed track between Naples and Rome, as the biggest share of the track runs through open field environments [7]. In general, an electrified HSR is characterized by the rails and the overhead line system. The overhead line system contains mainly of the masts, the support of the catenary and the catenary itself. Please note, that the type of masts for the overhead line system and signaling along the measured HSR were rectangular lattice masts. In addition, close buildings, e.g. electricity or cellular radio masts may appear sparsely as well as trees. A sketch of the environment is shown in Fig. 1. The red solid line indicates the line of sight (LOS) signal, whereas the blue dashed lines the multipath components (MPCs) scattered on the potential IOs.

Based on the architecture we define the position of the elements along the railway track and place masts, trees and

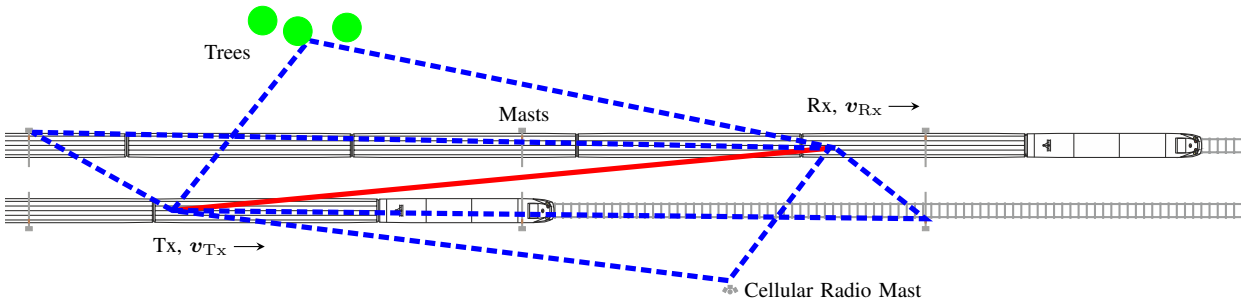

Fig. 1: Architecture of the open field environment.

close buildings for an open field environment. The actual position of each element can be set either by fixed values or can be based on derived statistics. For the first case with fixed position values, the positions of each element in x and y direction would reflect elements in the real measurement environment at the measurement campaign in Italy [3].

The second case allows the generation of an arbitrary setting within an open field environment; the x and y position of each element is estimated based on statistics. We derived these statistics by analyzing railway elements along the railway track for several kilometers. For example, the overhead line masts and the supports of the catenary appears regularly with a distance in x direction of $d_{\mathrm{M}} \in [32, 60]\,\mathrm{m}$; the average distance between the track and the masts in y direction is $3.4\,\mathrm{m}$ with a standard deviation of $0.14\,\mathrm{m}$ considering a double tracked HSR [5]. The amount of trees and and close buildings (e.g. cellular radio masts) is set randomly within a given boundary condition dependent on the total track length. Those elements are placed randomly to the left or right of the track. All placed elements along the railway track will be treated as IOs with the constrains of single bounce scattering or reflection.

IV. GSCM Implementation

The implementation of the GSCM follows several steps and results in a delay, Doppler-frequency and power representation of the propagation scenario.

A. Scenario

In addition to the architecture we need the following parameters to define a specific scenario for the GSCM. Firstly, we define a movement model of the transmitter (Tx) and the receiver (Rx) with arbitrary values for the velocities. Either a constant value is set for the whole simulation time, or the velocity changes over time. The velocity also describes the driving direction of the trains. In Fig. 1 we indicate the velocities and driving directions of the Tx and Rx. Secondly, we define the simulation time t_{sim}. The velocity and the simulation time result in the traveled distance of the Tx and Rx. Thirdly, we define the starting positions $\boldsymbol{T}(0)$ and $\boldsymbol{R}(0)$ of the Tx and the Rx, respectively. In Tab. I we show one example scenario which is reflecting one measurement scenario. In comparison to standard operational velocities of HSRs the velocities during the measurments had to be chosen very small because of the limitations of the measurement equipment [3]. Nevertheless, similar measurement evaluations in the field of T2G communications like in [8] state a negligible influence of the velocity no the stochastic parameters; only the Doppler frequency shift is related to the velocity and can be seen as a scaling factor. Hence, the proposed GSCM will support also higher velocities.

TABLE I: Open field scenario example.

Parameter	Unit	Setting
$\boldsymbol{v}_{\mathrm{Tx}}$	m/s	$[13.9, 0]^{\mathrm{T}}$
$\boldsymbol{v}_{\mathrm{Rx}}$	m/s	$[2.8, 0]^{\mathrm{T}}$
$\boldsymbol{T}(0)$	m	$[0, 2.5]^{\mathrm{T}}$
$\boldsymbol{R}(0)$	m	$[1000, -2.5]^{\mathrm{T}}$
t_{sim}	s	90

B. Delay and Doppler Frequency Representation

As a first step we can estimate the path lengths of the LOS signal and all MPCs. Based on the geometry of the given scenario, we can estimate the distances between the Tx and the Rx as LOS distance $d_{\mathrm{LOS}}(t) = \|\boldsymbol{R}(t) - \boldsymbol{T}(t)\|$ and between the Tx, all IOs $i = 1 \ldots N$ and the Rx as MPC distances $d_i(t) = \|\boldsymbol{R}(t) - \boldsymbol{IO}_i\| + \|\boldsymbol{IO}_i - \boldsymbol{T}(t)\|$ for each time instant t. Based on the distances we can derive the delay for the LOS signal

$$\tau_{\mathrm{LOS}}(t) = \frac{1}{\mathrm{c}} \|\boldsymbol{R}(t) - \boldsymbol{T}(t)\|\,, \tag{1}$$

and for the MPC as

$$\tau_i(t) = \frac{1}{\mathrm{c}} \left(\|\boldsymbol{R}(t) - \boldsymbol{IO}_i\| + \|\boldsymbol{IO}_i - \boldsymbol{T}(t)\|\right), \tag{2}$$

with the Tx position $\boldsymbol{T}$, the Rx position $\boldsymbol{R}$, the IO position $\boldsymbol{IO}_i$, and the speed of light c.

The Doppler frequency for the LOS signal is derived as

$$\nu_{\mathrm{LOS}}(t) = \frac{f_{\mathrm{c}}}{\mathrm{c}} \left(\boldsymbol{v}_{\mathrm{Rx}} - \boldsymbol{v}_{\mathrm{Tx}}\right) \frac{\boldsymbol{R}(t) - \boldsymbol{T}(t)}{\|\boldsymbol{R}(t) - \boldsymbol{T}(t)\|}, \tag{3}$$

and for the MPC as

$$\nu_i(t) = \frac{f_{\mathrm{c}}}{\mathrm{c}} \left(\boldsymbol{v}_{\mathrm{Rx}} \frac{\boldsymbol{R}(t) - \boldsymbol{IO}_i}{\|\boldsymbol{R}(t) - \boldsymbol{IO}_i\|} + \boldsymbol{v}_{\mathrm{Tx}} \frac{\boldsymbol{IO}_i - \boldsymbol{T}(t)}{\|\boldsymbol{IO}_i - \boldsymbol{T}(t)\|} \right), \tag{4}$$

with the velocitis $\boldsymbol{v}_{\mathrm{Tx}}$ and $\boldsymbol{v}_{\mathrm{Rx}}$, and the frequency f_{c}.

C. Power Representation

The complex received power is the superposition of all received signal components, i.e. the LOS signal and all MPCs. The individual complex power components are calculated as follows: The LOS signal power follows the log-distance path loss model presented in [4]. Hence, the received power can be derived as the product of the transmitted power, the log-distance path loss (PL) for the distance d_{LOS} including a shadow distribution $X_{\sigma_{\mathrm{PL}}}(t)$ and a phase term as

$$\begin{aligned} P_{\mathrm{r,LOS}}(t) =& P_{\mathrm{t}}\ \mathrm{PL}(d_0(t)) \left(\frac{d_{\mathrm{LOS}}(t)}{d_0(t)}\right)^{\frac{n(t)}{2}} X_{\sigma_{\mathrm{PL}}}(t) \\ & \times \exp\left(\frac{-\mathrm{j}2\pi d_{\mathrm{LOS}}(t)}{\lambda}\right). \end{aligned} \tag{5}$$

The power of a MPC received from a scattering IO is derived similar as the LOS signal power with one additional term for the scattering loss (SL) particular for one type of IO, e.g., an overhead line mast [5], as

$$\begin{aligned} P_{\mathrm{r},i}(t) =& P_{\mathrm{t}}\ \mathrm{PL}(d_0(t)) \left(\frac{d_i(t)}{d_0(t)}\right)^{\frac{n(t)}{2}} X_{\sigma_{\mathrm{PL}}}(t) \\ & \times \exp\left(\frac{-\mathrm{j}2\pi d_i(t)}{\lambda}\right) \\ & \times \left(\mathrm{SL}(\acute{d}_0(t)) \left(\frac{\acute{d}_i(t)}{\acute{d}_0(t)}\right)^{\frac{m(t)}{2}} X_{\sigma_{\mathrm{SL}}}(t)\right)^{-1}. \end{aligned} \tag{6}$$

The starting level of the PL model is set to $\mathrm{PL}(d_0(t)) = 10^{\mathrm{PL_{dB}}(d_0(t))/20}$ and similar for the SL model to $\mathrm{SL}(\acute{d}_0(t)) = 10^{\mathrm{SL_{dB}}(\acute{d}_0(t))/20}$. For both, the PL model and the SL model, the model exponents $n(t)$ and $m(t)$ are divided by a factor of two, as in (10) the received power in dBm of each received signal component is calculated by the square of the absolute power. In this way, the distance dependent trend of the time-variant received power remains correct. The distribution vector $X_\sigma(t)$ is a zero mean Gaussian vector with $\sigma = \{\sigma_{\mathrm{PL}}, \sigma_{\mathrm{SL}}\}$.

The received power of a MPCs caused by a reflection, e.g., a ground reflection or a reflection on a wall, is implemented as presented in [9] based on [10] as

$$\begin{aligned} P_{\mathrm{r},i}(t) =& P_{\mathrm{t}}\ \mathrm{PL}(d_0(t)) \left(\frac{d_i(t)}{d_0(t)}\right)^{\frac{n(t)}{2}} X_{\sigma_{\mathrm{PL}}}(t) \\ & \times \exp\left(\frac{-j2\pi d_i(t)}{\lambda}\right) \Gamma_i\left(\Theta(t)\right). \end{aligned} \tag{7}$$

TABLE II: Model parameters.

	Parameter	Unit	Setting
Open field	d_0	m	$[1, 100]^{\mathrm{T}}$
	$\mathrm{PL_{dB}}(d_0)$	dB	$[46.8, 86.8]^{\mathrm{T}}$
	n		$[2, 2.4]^{\mathrm{T}}$
	σ_{PL}	dB	$[2.6, 5.0]^{\mathrm{T}}$
Overhead line mast	$\acute{d}_0$	m	$[1, 4.4, 20, 60]^{\mathrm{T}}$
	$\mathrm{SL_{dB}}(\acute{d}_0)$	dB	$[5, 5, 21.4, 18.1]^{\mathrm{T}}$
	m		$[0, 2.5, -0.7, 0.7]^{\mathrm{T}}$
	σ_{SL}	dB	$[2.5, 5.3, 5.9, 5.9]^{\mathrm{T}}$
Close buildings	$\acute{d}_0$	m	1
	$\mathrm{SL_{dB}}(d_0)$	dB	22.4
	m		1
	σ_{SL}	dB	3.6
Trees	$\acute{d}_0$	m	1
	$\mathrm{SL_{dB}}(d_0)$	dB	22.9
	m		1
	σ_{SL}	dB	4.1
Ground reflection	ϵ_{r}		4.8
	Γ_i		$\Gamma_{\parallel}$
	h_{Tx}	m	4.1
	h_{Rx}	m	4.1

TABLE III: Channel sounder and measurement restrictions.

Parameter	Unit	Setting
f_{c}	GHz	5.2
B	MHz	120
t_{s}	ms	1.024
t_{p}	μs	12.8
P_{t}	dBm	27
t_{stat}	ms	65.5
f_{stat}	MHz	120

The wavelength is defined as $\lambda = \mathrm{c}/f_{\mathrm{c}}$. The reflection coefficient Γ_i depends on the incoming angle $\Theta(t)$ of the E-field and can either be parallel to the plane of incidence as

$$\Gamma_{\parallel}(\Theta(t)) = \frac{-\epsilon_{\mathrm{r}} \sin(\Theta(t)) + \sqrt{\epsilon_{\mathrm{r}} - \cos(\Theta(t))^2}}{\epsilon_{\mathrm{r}} \sin(\Theta(t)) + \sqrt{\epsilon_{\mathrm{r}} - \cos(\Theta(t))^2}}, \tag{8}$$

or perpendicular as

$$\Gamma_{\perp}(\Theta(t)) = \frac{\sin(\Theta(t)) - \sqrt{\epsilon_{\mathrm{r}} - \cos(\Theta(t))^2}}{\sin(\Theta(t)) + \sqrt{\epsilon_{\mathrm{r}} - \cos(\Theta(t))^2}}, \tag{9}$$

with the relative dielectric constant ϵ_{r} and $\Theta(t) = \tan^{-1}\left(\frac{d_i(t)}{h_{\mathrm{Tx}} + h_{\mathrm{Rx}}}\right)$ [10].

The measure of interest is the time-variant absolute received power in dBm. Hence, we can write

$$P_{\mathrm{r,dB}}(t) = 10 \log_{10} \left(\left| \begin{array}{c} P_{\mathrm{r,LOS}}(t) \\ P_{\mathrm{r},1}(t) \\ \vdots \\ P_{\mathrm{r,N}}(t) \end{array} \right|^2 \right). \tag{10}$$

V. Results

The GSCM provides the propagation characteristics in delay, Doppler frequency and power of the chosen scenario for each time instant t. We use the parameters listed in Tab. I and Tab. II to set up the simulation for the open field environment.

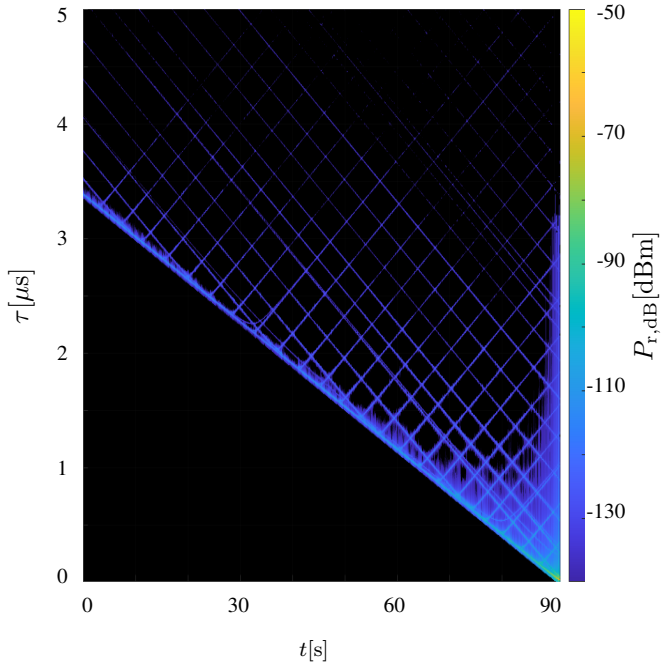

Fig. 2: PDP representation of the GSCM in open field environment.

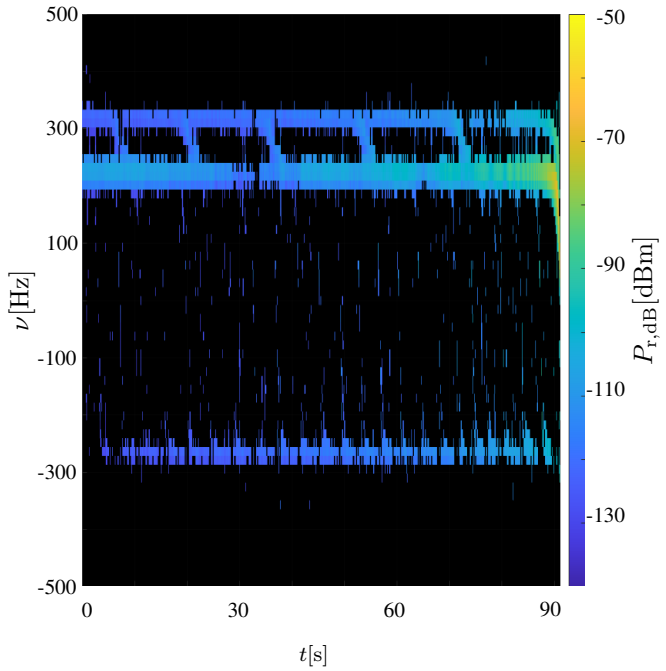

Fig. 3: DSD representation of the GSCM in open field environment.

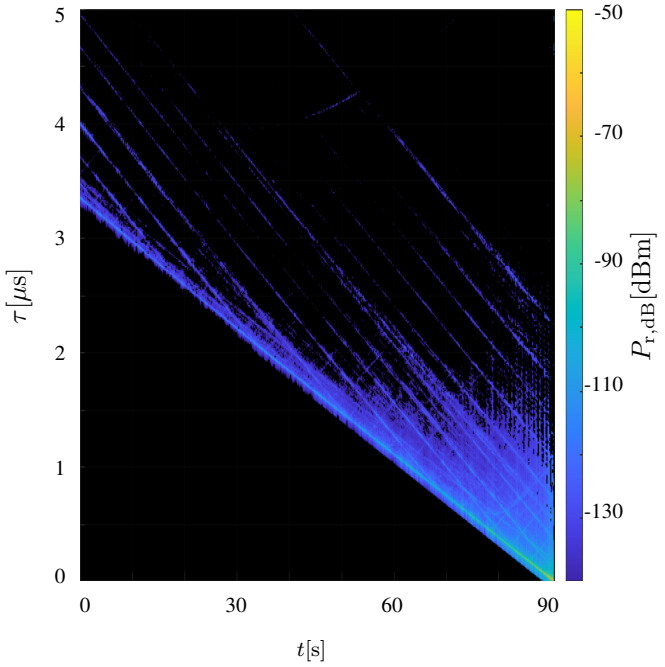

Fig. 4: PDP representation of the measurement data in open field environment.

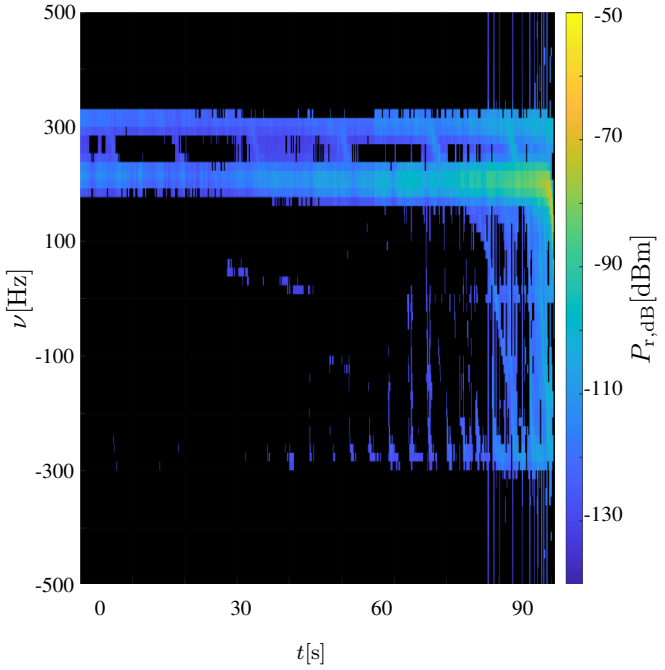

Fig. 5: DSD representation of the measurement data in open field environment.

The PL parameters are given for three distance segments and the SL parameters for either one or four distance segments. In detail, the GSCM uses different model parameters based on the distance d_{LOS} and d_i or uses a constant value for all distances. Hence, with the change of the distances the setting for some parameters may change over time.

We compare the outcome of the GSCM with the measurement results presented in [4]. To guarantee a fair comparison we apply the same restrictions to the GSCM as the measurements experience due to the used DLR RUSK channel sounder.

Hence, we superimpose the outcome of the GSCM with a Dirichlet function to result in a circular sinc representation in the delay and Doppler frequency domain. Furthermore, we apply the same quasi-stationarity assumptions as used in the measurement data analysis in [4]. To avoid noise bias in the results, we estimated the noise floor for each time-instant t and removed all values that were smaller than $3\,\mathrm{dB}$ above the noise floor. All restrictions are listed in Tab. III.

We combine the delay and power characteristics to a time-variant PDP representation and show the outcome of the GSCM in Fig. 2. In Fig. 4 we show the equivalent scenario from the measurement campaign: Both trains are driving in the same direction on parallel tracks and the Tx approaches the Rx. As a consequence the delay of the LOS signal decreases from $3.34\,\mu\mathrm{s}$ at $t = 0\,\mathrm{s}$ to $16.7\,\mathrm{ns}$ at $t = 90\,\mathrm{s}$. We perform the same comparison for the Doppler frequency and power characteristics in the form of the time-variant DSD shown in Fig. 3 and Fig. 5 for the GSCM and the measurement results, respectively.

For both, the delay and Doppler frequency representations we see a good match between the GSCM and the measurement data. The PDP of the GSCM data clearly shows a regular grid of MPCs in Fig. 2. The regular shape reflects the regular spacing of overhead line masts. The MPCs caused by IOs in-front of the train are similar visible as the ones from IOs in the back of the train. The GSCM is considering a perfectly omni-directional antenna pattern and therefore, no angular dependent weight is added. In comparison, in Fig. 4 we clearly see pronounced MPCs with a decreasing trend in delay and less pronounced MPCs with an increasing trend in delay. The MPCs caused by IOs behind both trains, in other words MPCs with an increasing trend in delay, experience an attenuation due to the antenna pattern of the antennas used during measurements [3].

The same behavior is reflected in the DSD representation; in Fig. 5 the received power is lower for MPCs with $\nu \approx -300\,\mathrm{Hz}$ compared to the same area of MPCs in Fig. 3. For the MPCs with a positive Doppler frequency, i.e. MPCs caused by IOs in-front of the trains with $\nu \approx 300\,\mathrm{Hz}$, and for the LOS signal at $\nu \approx 200\,\mathrm{Hz}$ the received power values of the GSCM agree with those of the measurements. In Fig. 3 and Fig. 5 we clearly see the discretization due to the channel sounder limitations. The stationarity window of $t_{\mathrm{stat}} = 65.5\,\mathrm{s}$ results in a Doppler frequency resolution of $15.26\,\mathrm{Hz}$ [4]. Due to the long measurement time of $t = 90\,\mathrm{s}$ the discretization of $t_{\mathrm{s}} = 1.024\,\mathrm{ms}$ is hardly visible.

VI. Conclusion

In this publication we presented a GSCM for T2T communication. The GSCM combines railway scenarios for future railway applications, e.g., virtual coupled trains with measurement based propagation characteristics. The investigation of propagation characteristics for typical railway environments and railway elements along the railway track were presented in previous publications. We showed the implementation on the example of an open field environment and two trains running on parallel tracks. The output of the GSCM in form of a delay, Doppler frequency and power representation was compared to measurement results in a equivalent environment and scenario. We performed a qualitative validation of the model based on the PDP and DSD and found a good match between the model and the measured data.

Based on the presented implementation of the GSCM we will introduce more typical elements along the railway track and will add additional railway environments to the model. Future quantitative validations will confirm the presented results of the proposed GSCM for T2T communication. Different movements of the trains, the elements along the track and typical environments can be arbitrary combined within the GSCM. As a result, different scenarios can be generated and provided. In comparison to poor stochastic channel models, the GSCM can be used to investigate the influence of temporal correlation effects on the wireless communication for safety critical railway applications. The final GSCM will be a powerful tool for system testing or for the development of future communication standards in the railway domain.

References

[1] J. Moreno García-Loygorri, J. Goikoetxea, E. Echeverria, A. Arriola, I. Val, S. Sand, P. Unterhuber, and F. del Rio, "The wireless train communication network: Roll2rail vision," *IEEE Vehicular Technology Magazine*, vol. 13, no. 3, pp. 135–143, 09 2018.

[2] P. Unterhuber, S. Pfletschinger, S. Sand, M. Soliman, T. Jost, A. Arriola, I. naki Val, C. Cruces, Moreno García-Loygorri, J. García-Nieto, C. Rodríguez, M. Berbineau, E. Echeverría, and I. Baz, "A Survey of Channel Measurements and Models for Current and Future Railway Communication Systems," *Mobile Information Systems*, vol. 2016, pp. 1–14, June 2016. [Online]. Available: http://dx.doi.org/10.1155/2016/7308604

[3] P. Unterhuber, S. Sand, M. Soliman, B. Siebler, A. Lehner, T. Strang, M. d'Atri, F. Tavano, and D. Gera, "Wide Band Propagation in Train-to-Train Scenarios - Measurement Campaign and First Results," in *11th European Conference on Antennas and Propagation (EuCAP)*, March 2017, pp. 3356–3360.

[4] P. Unterhuber, M. Walter, U.-C. Fiebig, and T. Kürner, "Stochastic channel parameters for train-to-train communications," *IEEE Open Journal of Antennas and Propagation*, vol. 2, pp. 778–792, July 2021.

[5] P. Unterhuber, M. Walter, and T. Kürner, "Influence of railway infrastructure on train-to-train communications," in *15th European Conference on Antennas and Propagation (EuCAP)*, April 2021, pp. 1–5.

[6] Trenitalia, "ETR 500," 2021. [Online]. Available: www.trenitalia.com/en/frecce/frecciarossa_etr500.html

[7] Wikipedia, "Rome–Naples high-speed railway," 2021. [Online]. Available: en.wikipedia.org/wiki/Rome%E2%80%93Naples_high-speed_railway

[8] T. Domínguez Bolaño, *Design and evaluation of new waveforms for high mobility communications*, A Coruña, Sep. 2018.

[9] P. Unterhuber, I. Rashdan, M. Walter, and T. Kürner, "Path loss models and large scale fading statistics for c-band train-to-train communication," in *14th European Conference on Antennas and Propagation (EuCAP)*, April 2020, pp. 1–5.

[10] T. S. Rappaport, *Wireless Communications: Principles and Practice*, ser. Prentice Hall communications engineering and emerging technologies series. Prentice Hall PTR, 2002.